Rotational magnetic endosome microrheology: Viscoelastic architecture inside living cells

C. Wilhelm, F. Gazeau, and J.-C. Bacri
Laboratoire des Milieux Désordonnés et Hétérogènes, UMR7603 FR2438 "Matière et Systèmes Complexes," Université Pierre et Marie Curie, Tour 13, Case 86, 4 Place Jussieu, 75005 Paris, France
(Received 28 December 2002; revised manuscript received 28 February 2003; published 23 June 2003)

The previously developed technique of magnetic rotational microrheology [Phys. Rev. E **67**, 011504 (2003)] is proposed to investigate the rheological properties of the cell interior. An endogeneous magnetic probe is obtained inside living cells by labeling intracellular compartments with magnetic nanoparticles, following the endocytosis mechanism, the most general pathway used by eucaryotic cells to internalize substances from an extracellular medium. Primarily adsorbed on the plasma membrane, the magnetic nanoparticles are first internalized within submicronic membrane vesicles (100 nm diameter) to finally concentrate inside endocytotic intracellular compartments (0.6 μm diameter). These magnetic endosomes attract each other and form chains within the living cell when submitted to an external magnetic field. Here we demonstrate that these chains of magnetic endosomes are valuable tools to probe the intracellular dynamics at very local scales. The viscoelasticity of the chain microenvironment is quantified in terms of a viscosity η and a relaxation time τ by analyzing the rotational dynamics of each tested chain in response to a rotation of the external magnetic field. The viscosity η governs the long time flow of the medium surrounding the chains and the relaxation time τ reflects the proportion of solidlike versus liquidlike behavior ($\tau = \eta/G$, where G is the high-frequency shear modulus). Measurements in HeLa cells show that the cell interior is a highly heterogeneous structure, with regions where chains are embedded inside a dense viscoelastic matrix and other domains where chains are surrounded by a less rigid viscoelastic material. When one compound of the cell cytoskeleton is disrupted (microfilaments or microtubules), the intracellular viscoelasticity becomes less heterogeneous and more fluidlike, in the sense of both a lower viscosity and a lower relaxation time.

DOI: 10.1103/PhysRevE.67.061908 PACS number(s): 87.16.Ka, 87.16.Tb, 83.85.Cg, 75.50.Mm

I. INTRODUCTION

Cell viscoelasticity and its ability to withstand applied stress are crucial to explain cellular functions (cell division, muscle contraction, cell adhesion, cell spreading), motivating, for almost three decades, the large number of studies that have focused on determining the rheological behavior of living cells. Whole-cell deformation has been achieved using different techniques: (i) fluid shear or centrifugal forces [1] have been used to apply a global load to the cell; (ii) micropipet aspiration [2] has been the main assay to measure both the elastic modulus of the cell membrane and the viscoelastic properties of the cell interior [3–5]; (iii) microplate manipulation [6] has been used to impose uniaxial deformation on an individual cell, allowing time scale measurements of its structural properties; and (iv) the concept of optical deformability was more recently used to deform the cell with an optical stretcher [7]. At a smaller scale, the cell was probed through its surface by manipulation with microneedles [8], cell poking [9], and atomic force microscopy, with recent improvements for cell elasticity measurements by attaching a microsphere to the end of the scanning tip [10,11]. Microspheres attached on the cell surface have commonly been used to measure the specific viscoelastic coefficients of the plasma membrane using optical tweezers [12] or magnetic bead rheometry [13], and more recently to deduce the whole frequency dependent mechanical behavior of the cortical cytoskeleton [14,15]. However, until now, only a few attempts to measure the local viscoelasticity inside the cell have been developed, following two distinct approaches. On one hand, spontaneous motion and diffusion of intracellular organelles such as granules [16] or engulfed microspheres [17] are used to investigate the cell interior. On the other hand, intracellular granules trapped with optical tweezers [18] or phagocytosed magnetic microspheres rotated [19,20] and translated [21] by external fields enable one to transmit stress directly to the cytoplasm, allowing investigations of the cytoskeletal mechanics. The magnetic intracellular probe then depends on the process of phagocytosis, during which a specialized cell is able to internalize micrometer-sized particles. Nevertheless, the common way to ingest extracellular material for all eucaryotic cells consists in the process of endocytosis in which portions of the plasma membrane invaginate and pinch off to form an intracellular vesicle containing the ingested substance. The primary endocytotic vesicles formed exhibit diameters from 50 to 100 nm, making it impossible for a micrometric bead to follow this specific way. By contrast, nanometer-sized magnetic particles follow this endocytosis pathway: nanoparticles are delivered from the first endocytotic vesicles into larger organelles, namely, endosomes, which are micrometer-sized intracellular vesicles (0.6 μm diameter). We are then able to obtain a magnetic probe inside nonphagocyting cells by labeling these preexisiting intracellular compartments with magnetic nanoparticles. Magnetic endosomes loaded with nanoparticles attract each other and align to form chains inside the cell, when they are submitted to an external magnetic field. The chains of magnetic endosomes appear as suitable tools to probe the viscoelasticity of the cytoplasm using the new rotational microrheological technique described in [22]. It consists in analyzing the response of the chains to a controlled applied magnetic torque. Relevant results concerning

the local microenvironment of endocytotic organelles are found by performing the viscoelastic measurements on a general mammalian cell model (HeLa cells), inside cells with an intact cytoskeleton or inside cells where one of the cytoskeleton compounds, microtubules or actin filaments, is selectively disrupted.

II. MATERIALS AND METHODS

A. Cell culture and magnetic labeling

HeLa human ovarian tumor cells were grown at 37 °C in 5% CO_2 in Dulbecco's modified Eagle medium supplemented with 10% heat inactivated fetal calf serum, 50 units/ml penicillin, 40 mg/ml streptomycin and 0.3 mg/ml L-glutamine in specially designed 1 mm cylindrical chambers stuck on glass circular lamellae to which cells adhere. Magnetic cell labeling was achieved using cobalt ferrite magnetic nanoparticles ($CoFe_2O_4$). The nanoparticles have a mean diameter of 8 nm and bear negative charges due to carboxylate groups complexed on their surface, ensuring their stability in aqueous solution. Each nanoparticle is a ferrimagnetic single domain with a mean magnetic moment of 1.2×10^{-19} A m^2. They are dispersed in serum-free culture medium with a corresponding iron concentration [Fe] $=10$ mM and are incubated with HeLa cells for 1 h, followed by a 1 h chase, both steps at 37 °C. Nanoparticle cell uptake was quantified through the magnetophoresis assay [23], where the velocity of a cell in suspension submitted to a magnetic field gradient leads to the amount of internalized nanoparticles by simply balancing magnetic and viscous forces. For the above incubation conditions, each cell internalizes a mean number of $(11\pm2.7)\times10^6$ nanoparticles per cell (corresponding to 21.4 ± 5.2 pg of iron per cell).

B. Electron microscopy

After the magnetic labeling and chase, adhering cells were washed twice with 0.1M cacodylate buffer and then fixed in 2% glutaraldehyde in cacodylate buffer for 1 h at 4 °C. Cells were then postfixed in 1% OsO_4 for 2 h at 4 °C, washed again with cacodylate buffer, dehydrated in an alcohol series, and embedded in Epon. Ultrathin sections of 70 nm were examined with a JEOL120CX transmission electron microscope. In some cases, a 100 mT homogeneous magnetic field was applied in the plane of the cell monolayer for 15 min before and 15 min after glutaraldehyde addition.

C. Immunofluorescence microscopy and cytoskeletal drugs

Fluorescent labeling of the cytoskeletal networks of filamentous actin and of microtubules was achieved using, respectively, phalloidin and antitubulin antibody. Cells were fixed under a 100 mT magnetic field with 3% paraformaldehyde in phosphate buffer saline (PBS), permeabilized with PBS containing 0.1% saponin and labeled with rhodamine phalloidin or with an antitubulin antibody revealed with a conjugated secondary antibody. The cells were then observed with a confocal laser-scanning microscope. Latrunculine A and nocodazole were used to depolymerize, respectively, the actin filaments and the microtubules. The cells were incubated for 10 min with latrunculine A at 1 μM or 30 min with nocodazole at 10 μM. The effect of the drugs was observed for each type of filament by immunofluorescence on the cells fixed under a magnetic field.

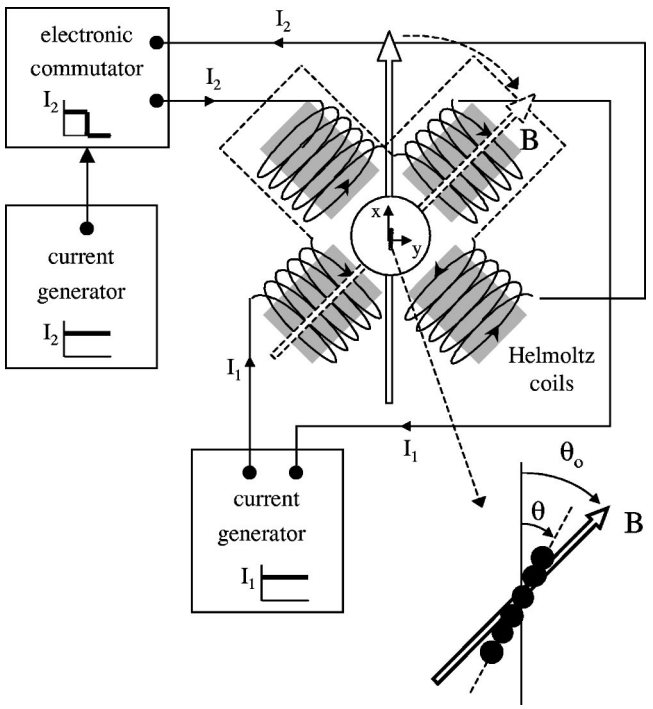

FIG. 1. Magnetic device to perform microrheological measurements inside the cell. Two pairs of coils in the Helmholtz configuration are supplied with the same current intensity, providing a magnetic field along the x direction. The intensity of the pair of coils parallel to the $(x,-y)$ diagonal can be switched to zero in a characteristic time smaller than 1 μs by using an electronic commutator. Thus, the magnetic field can be rotated quasi-instantaneously at $t=0$ from the x direction ($\theta=0$) toward the direction $\theta=\theta_0=45°$. The probe—chain of magnetic endosomes—then experiences an initial magnetic torque proportional to the magnetic field B created by the pair of coils parallel to the (x,y) diagonal, and its subsequent rotation is parametrized by the angle θ, varying from $\theta=0$ to $\theta=\theta_0$.

D. Magnetic device under microscope

To magnetically monitor the magnetic endosomes inside the cells, the magnetic field setup shown in Fig. 1 was adapted to an inverted Leica microscope with a plan 100× oil immersion thermostated lens. Two pairs of Helmholtz coils are positioned on the two diagonals of the microscope plane. A permanent current supplies one pair of coils, creating a homogeneous magnetic field B in the (x,y) diagonal. Measurements were performed using four different values of the magnetic field B: 23, 32.5, 39, and 55 mT (corresponding to currents from 2 to 5.5 A). The other pair of coils, along the $(x,-y)$ diagonal, is supplied by the same current that goes through an electronic commutator allowing one to switch off the current in it with a characteristic time lower than 1 μs. The magnetic field resulting from both pairs of Helmholtz

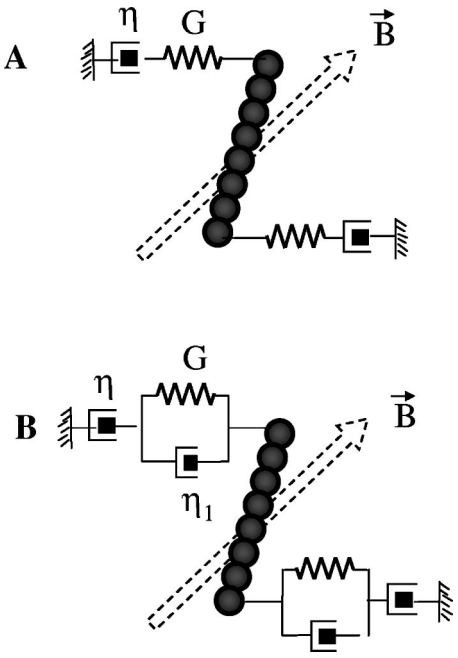

FIG. 2. Mechanical equivalent circuits to describe the behaviors of (a) a typical linear Maxwell fluid (elastic spring G associated in series with a dashpot η) and (b) the cell interior viscoelasticity [elastic Voigt element (parallel arrangement of a spring G and a dashpot η_1) in series with a dashpot η].

coils is first oriented along the x direction (defining $\theta=0$) and rotates quasi-instantaneously toward the direction $\theta_0=45°$, when the current in the second pair of coils is switched off. Both pairs of coils are thermostated to avoid overheating. The 10 mm diameter cylindrical chambers containing cells are placed inside the coils. The entire device is regulated at 37 °C. All the images were captured using an ultrafast camera and digitized on a computer. The video system samples up to 500 images per second. The probe rotation is analyzed using a self-written tracking algorithm implemented with NIH image-processing software.

III. PRINCIPLES

Rotational microrheology

Soft materials often display characteristics of both fluids and solids. Their viscoelastic properties reflect their ability to dissipate (viscosity) and to store (elasticity) mechanical energy at the same time. To describe the combined viscous and elastic properties of such systems, one simple model consists in adopting a mechanical equivalent circuit of a viscous dashpot and an elastic spring in series, as represented in Fig. 2(a) (Maxwell model). The local viscoelasticity can be deduced from the rotational dynamics of a small probe inserted inside the considered medium. Probe rotation (angle of rotation θ) is induced by the applied torque Γ, which is counteracted by the viscous torque (proportional to $d\theta/dt$) and the elastic torque (proportional to θ) exerted by the medium on the probe. The angular velocity is therefore the sum of a viscous contribution and an elastic one:

$$\frac{d\theta}{dt}=\frac{\Gamma}{\kappa V\eta}+\frac{1}{\kappa VG}\frac{d\Gamma}{dt}, \tag{1}$$

where V is the volume of the probe and κ the rotational factor depending on the probe geometry. η and G are, respectively, the viscosity and the elasticity of the surrounding medium. One can define the relaxation time τ:

$$\tau=\frac{\eta}{G}, \tag{2}$$

which is a measure of the time required for stress relaxation. This relaxation time is a convenient independent parameter to quantify the extent of fluidlike versus solidlike behaviors of the material: a purely elastic medium is characterized by $\tau=\infty$, whereas a purely fluid medium is characterized by $\tau=0$.

The probes used in this study are magnetic endosomes chained in the direction of an applied magnetic field. At $t=0$, the permanent magnetic field is instantaneously rotated through an angle θ_0 with respect to its initial x direction (see Fig. 1 for angle notations). The kinetics of the resulting rotation of each chain depends on the local viscoelasticity surrounding it. For such a probe geometry, it was demonstrated [22] that the geometrical factor κ follows a phenomenological law for any size of chain: if N is the number of magnetic microspheres per chain,

$$\kappa(N)=\frac{2N^2}{\ln(N/2)+2.4/N}. \tag{3}$$

For magnetic endosomes exhibiting a paramagnetic behavior, the magnetic torque exerted on a chain of N endosomes, under the effect of an external magnetic field B making an angle $(\theta_0-\theta)$ with the chain orientation, has been calculated in [24] and is written

$$\Gamma=\kappa_m V\frac{\sin[2(\theta_0-\theta)]}{2}, \tag{4}$$

where κ_m is defined as

$$\kappa_m(N)=\frac{1}{8\mu_0}N\chi^2B^2. \tag{5}$$

μ_0 is the vacuum permeability constant and χ is the magnetic susceptibility of the endosomes, defined as the fraction of their volume magnetization $M_e(B)$ over the field B:

$$\chi(B)=\mu_0\frac{M_e(B)}{B}. \tag{6}$$

With the applied magnetic torque given in Eq. (4), the chain dynamics in a fluid having a linear Maxwellian rheological behavior [Eq. (1)] becomes

$$\frac{d\theta}{dt}=\frac{\kappa_m}{2\kappa}\frac{1}{\eta}\left(\sin[2(\theta_0-\theta)]+\tau\frac{d}{dt}\{\sin[2(\theta_0-\theta)]\}\right). \tag{7}$$

To describe the rheological properties of the cell interior, we consider an extension of the Maxwell mechanical circuit (Voigt-Maxwell body) as represented in Fig. 2(b). A Voigt element (parallel arrangement of a spring G and a dashpot η_1) accounts for the solidlike behavior whereas the dashpot η accounts for the liquidlike behavior. In this case, the rotation of the probe is governed by Eq. (8):

$$\frac{\eta_1}{G}\frac{d^2\theta}{dt^2}+\frac{d\theta}{dt}=\frac{\Gamma}{\kappa V\eta}+\frac{1}{\kappa VG}\left(1+\frac{\eta_1}{\eta}\right)\frac{d\Gamma}{dt}, \qquad (8)$$

where Γ is the magnetic torque defined in Eq. (4). For a chain rotating toward a magnetic field at θ_0 from the initial chain orientation, the motion equation is written as

$$\tau_1\frac{d^2\theta}{dt^2}+\frac{d\theta}{dt}=\frac{\kappa_m}{2\kappa}\frac{1}{\eta}\left(\sin[2(\theta_0-\theta)]+(\tau+\tau_1)\frac{d}{dt}\{\sin[2(\theta_0-\theta)]\}\right). \qquad (9)$$

κ and κ_m are given by Eqs. (3) and (5), η is the viscosity, $\tau_1=\eta_1/G$ is the lag time due to the Voigt element (time required for the extension of the spring to its equilibrium), and $\tau=\eta/G$ is the relaxation time. Figure 3 shows typical response curves obtained by resolving Eq. (9) numerically for different sets of viscoelastic parameters. The viscosity η governs the long time viscous flow behavior [Fig. 3(a)] and the shear modulus G the initial fast elastic jump [Fig. 3(c)]. The lower the viscosity η_1, the faster is the initial elastic jump (the limit $\eta_1=0$ corresponding to the Maxwell behavior, instantaneous jump) [Fig. 3(b)].

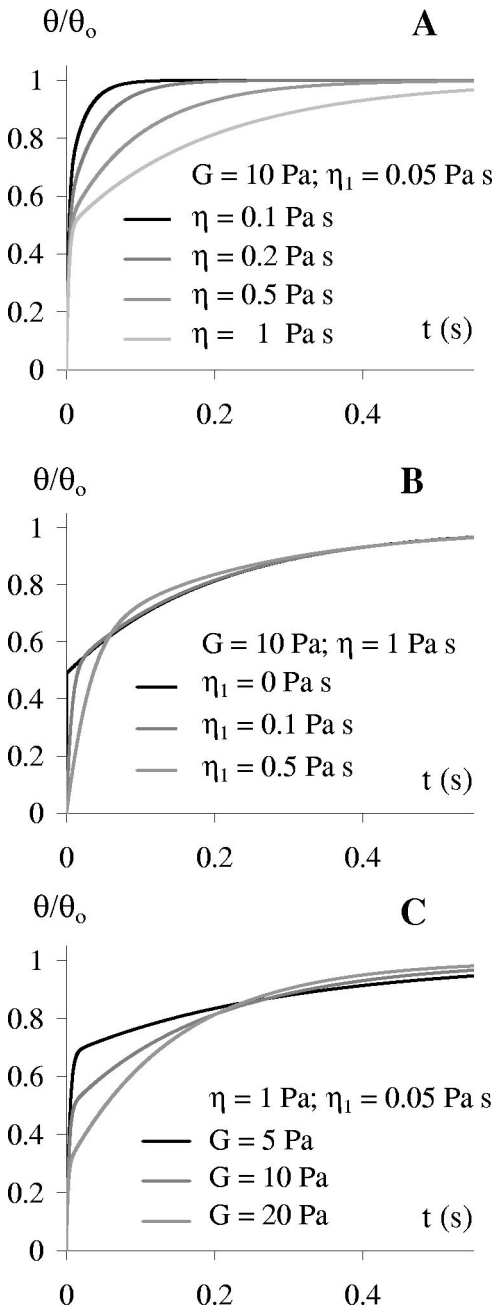

FIG. 3. Theoretical curves calculated numerically from Eq. (9) for a presumed chain of three magnetic endosomes rotating toward a $B=39$ mT magnetic field oriented along the $\theta=\theta_0$ direction. One can observe the separate effects of the viscosities η and η_1 and of the shear modulus G.

IV. RESULTS

A. Formation of magnetic endosomes in living cells: Chaining effect under magnetic field

Magnetic nanoparticles, owing to their tiny volume and negative surface charges, present a high nonspecific affinity for the plasma membrane of various cells, probably of electrostatic origin. Nanoparticle adsorption on the plasma membrane triggers their internalization within endocytotic vesicles, following the endocytosis pathway. The different steps of nanoparticle endocytosis and the cytoplasmic localization of magnetic compartments have been fully characterized in [25]. Electron micrographs of labeled cells show that after the whole incubation (1 h) and chase (1 h) process, the nanoparticles, which are dark to electrons, are densely confined within membrane bound organelles, likely late endosomes or lysosomes, of mean diameter $d=0.6$ μm [Fig. 4(a)].

Submitted to an external homogeneous magnetic field B, endosomes loaded with iron oxide nanoparticles attract each other via dipole-dipole magnetic interactions and form chains inside the cytoplasm along the direction of the field. Such endosome chaining can be seen on electron micrographs of cells that are fixed under a 100 mT magnetic field [Fig. 4(b)]. Chains containing from two to ten endosomes (1 to 6 μm long) are observed throughout the cytoplasm. Note that, along the chain, each magnetic endosome stays a distinct entity. By transmission light microscopy, chains of magnetic endosomes appear as black bars inside the cells [Fig. 4(c)]. The combined observations of chains inside the cells and cytoskeleton networks show that the chaining effect does not perturb either actin filaments or microtubule architecture: no anisotropic structure of the filaments that correlates to the chain orientation is revealed [Fig. 5(a)]. In addition, once they are formed in the entire cell, endosome chains are stable

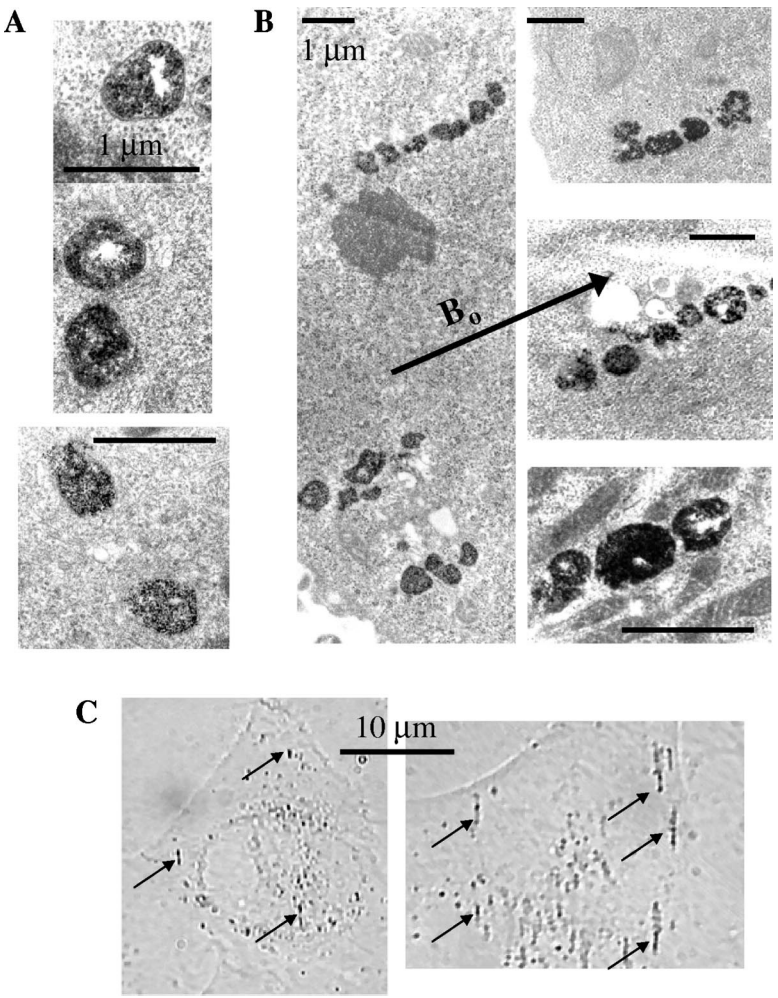

FIG. 4. (a) Electron micrographs representing parts of the cytoplasm of HeLa cells after 1 h incubation at 37 °C with magnetic nanoparticles ([Fe] = 10 m*M*) followed by 1 h chase. The nanoparticles (black points) are confined within endosomes, dispersed throughout the cell cytoplasm. (b) Electron micrographs of HeLa cells after 1 h incubation at 37 °C with magnetic nanoparticles ([Fe] = 10 m*M*) followed by 1 h chase (including 30 min under a homogeneous magnetic field $B_0 = 100$ mT). Chains of magnetic endosomes are observed along the magnetic field direction. (c) Living HeLa cell light transmission images. Chains of magnetic endosomes (pointed out with solid arrows) are oriented along the *x* direction of the magnetic field created by the two pairs of Helmholtz coils (see the setup in Fig. 1).

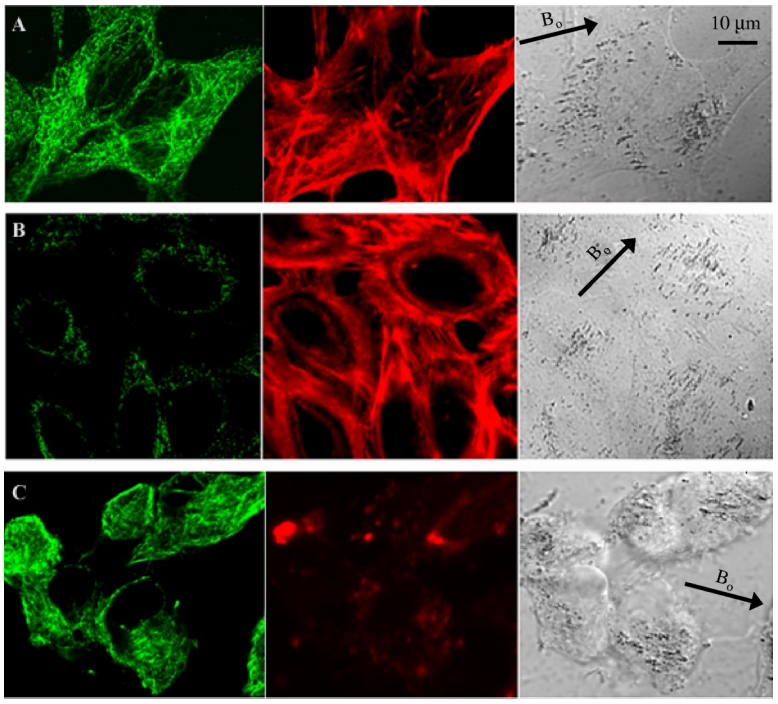

FIG. 5. (Color online) Effect of drugs that selectively disorganize filaments of the cytoskeleton. The same cells are labeled with antitubulin antibody (left) and fluorescent phalloidin (center) and are observed with a confocal microscope [direct image (right)]. Cells are fixed when submitted to a magnetic field $B_0 = 100$ mT. (a) Control cells. (b) Cells treated for 30 min with 10 μM nocodazole. (c) HeLa cells treated for 10 min with 1 μM latrunculine A.

under magnetic field with respect to the further disruption of actin filaments or microtubules using cytoplasmic drugs [Figs. 5(b) and 5(c)].

B. Chains of magnetic endosomes as probes for the viscoelasticity: Validation and calibration

The rotational microrheology technique described in Sec. III has been validated in a typical Maxwell fluid in [22] using 0.65 μm paramagnetic microspheres made of iron oxide nanoparticles dispersed in low density polystyrene. To demonstrate that chains of magnetic endosomes, as well, are suitable probes for viscoelasticity, the magnetic properties of the magnetic endosomes must be determined, and the rotation of chains of magnetic endosomes must be monitored inside the previously investigated Maxwell fluid. Intracellular magnetic endosomes must therefore be extracted from the cell inside: Cells were mechanically lysed in a 250 mM sucrose medium, the postnuclear supernatant (PNS) obtained after centrifugation and the magnetic endosomes isolated from the rest of the PNS through a magnetic column (high magnetic field gradient). First, the magnetization curve of a known number of the purified magnetic endosomes, obtained using a superconducting quantum interference device (SQUID), shows that the magnetic endosomes exhibit a superparamagnetic behavior, acquiring a global magnetization per unit volume $M_e(B)$ under a magnetic field B, with no magnetic hysteresis (the nanoparticles are consequently free to rotate within the surrounding endosome lumen). Each endosome of mean diameter d carries a magnetic moment $m_e(B) = (\pi/6)d^3 M_e(B)$. The saturation magnetization at 5 T yields to a mean saturating magnetic moment of 6.2×10^{-15} A m^2 for an endosome, equivalent to a content of about 5.2×10^4 nanoparticles per endosome, occupying a volume fraction of 24%. Second, the purified magnetic endosomes are dispersed inside the Maxwell fluid, at a volume fraction of 0.07%. This fluid consists of a solution of surfactant molecules cethyltrimethyl ammonium chloride (CTAC) in water, forming cylindrical micelles which entangle and confer viscoelastic properties on the system. The micellous solution has been previously characterized with a Couette rheometer at a fixed temperature of 30 °C, demonstrating a Maxwell behavior with the viscosity $\eta = 3.5$ Pa s and the shear modulus $G = 59$ Pa (relaxation time $\tau = 0.06$ s). Chains of magnetic endosomes are formed within this viscoelastic fluid, and the rotation of chains containing N endosomes (N varying from 2 to 8) is measured as a function of time [Fig. 6(a)]. Experimental points are well adjusted using Eq. (7), which is characteristic of Maxwell behavior. The magnetic factor is calculated from Eq. (5), where the magnetic susceptibility χ for the applied field B is measured on the magnetization curve of the endosomes. The best adjustments [solid curves in Fig. 6(a)] are obtained for a viscosity $\eta = 3.5 \pm 0.2$ Pa s, a relaxation time $\tau = 0.06 \pm 0.005$ s, and a geometrical factor κ varying with the number N of endosomes in the chain as represented in Fig. 6(b). These viscoelastic parameters are in good agreement with the parameters deduced from conventional rheological measurements. Moreover, the geometrical factor κ varies with N as predicted by Eq. (3) [see the solid line in Fig. 6(b)]. This assay with a known viscoelastic fluid definitely validates the use of chains of magnetic endosomes, with different lengths, to probe the viscoelasticity of their surrounding medium.

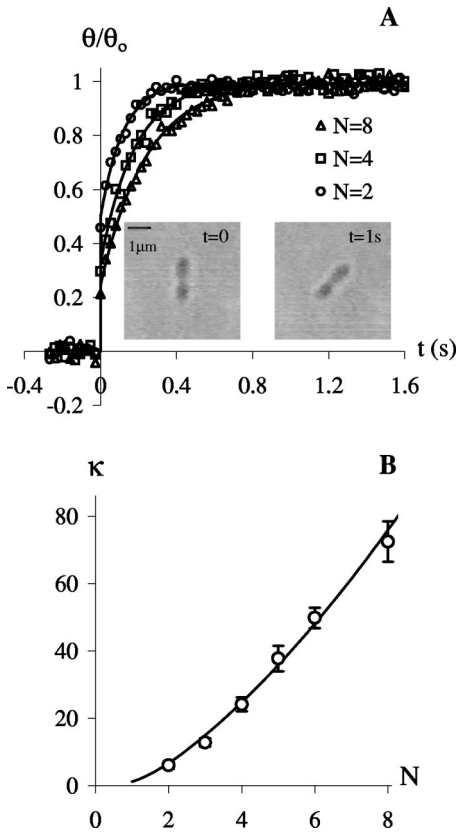

FIG. 6. Calibration of the rotational microrheology assay with chains of magnetic endosomes as probes. (a) Rotation of chains of N endosomes inside a linear viscoelastic fluid under the effect of a step magnetic field applied at $t = 0$, making an angle of 45° with respect to the initial chain orientation. Initial and final chain orientations are illustrated in the insets for a chain of four endosomes. The solid curves represent the optimal adjustment of the experimental points with Eq. (6) and correspond to the rheological behavior of a Maxwell viscoelastic fluid. (b) Validation of the geometrical factor governing the torque applied on the chains by the fluid. Experimental points (circles) are well described by the phenomenological law (solid line) defined in Eq. (3).

C. Measurement of local viscoelasticity in the cell cytoplasm

Figures 7(a) and 7(b) shows typical rotational response curves for chains of magnetic endosomes within HeLa cells. The rotation time varies from several seconds [Fig. 7(a)] to a few tenths of seconds [Fig. 7(b)]. When one member of the cytoskeleton network is deleted, actin filaments [Fig. 7(c)] or microtubules [Fig. 7(d)], all the chains rotate with approximately the same characteristic time of the order of a few tenths of seconds. For all cases, the response curves exhibit two regimes, reflecting a Maxwell-like behavior (effective viscosity and elasticity associated in series): a fast elastic deflection followed by a long time viscous behavior. The initial elastic response occurs with a nonzero characteristic time τ_1, eliminating therefore a description with a simple

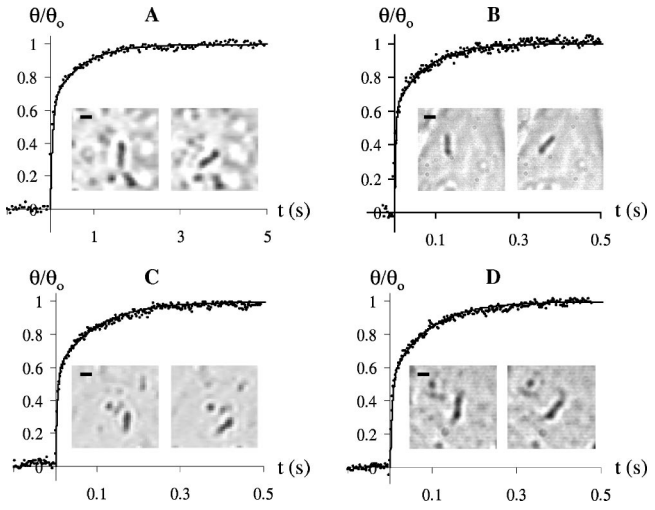

FIG. 7. Examples of angular response curves for two different chains inside cells with intact cytoskeleton: chain can rotate either in a few tenths of seconds (a) or in a few seconds (b), depending on its intracellular localization. Typical angular response curves for a chain inside a cell where actin filaments have been disrupted (c) or where microtubules have been disrupted (d). The best fits are represented by solid lines and correspond to the viscoelastic parameters $\eta=1.8$ Pa s, $\tau=0.36$ s, $\tau_1=0.026$ s (a); $\eta=0.35$ Pa s, $\tau=0.044$ s, $\tau_1=0.009$ s (b); $\eta=0.6$ Pa s, $\tau=0.1$ s, $\tau_1=0.008$ s (c); $\eta=0.32$ Pa s, $\tau=0.043$ s, $\tau_1=0.009$ s (d). Representative observations of the chains just before the instantaneous rotation of the field (chains are along the vertical direction) and after the rotation of the chains (chains are oriented at $\theta=\theta_0=45°$ from the vertical direction) are superimposed on the plots (bar$=1$ μm).

Maxwell model. Then the chains attain the direction of the permanent field with the relaxation time τ. The arrangement of rheological mechanical elements represented in Fig. 2(b) (also called a Voigt-Maxwell body) is the simplest configuration that explains the experimental curves. It consists of a Voigt element (parallel arrangement of a spring G and a dashpot η_1) accounting for the solidlike behavior at short times, in series with a dashpot η responsible for the liquidlike behavior at longer times. η represents the effective viscosity of the network surrounding the chains, $\tau=\eta/G$ is the effective relaxation time [equivalent to the Maxwell viscoelastic time defined in Eq. (2)] which controls the establishment of the long time viscous flow regime, and $\tau_1=\eta_1/G$ is the characteristic time measuring the establishment of the initial elastic stress (η_1 reflects the finite initial flow). With this configuration, the chain dynamics is described by Eq. (9), which fits the experimental curves with very good agreement (see the solid lines in Fig. 7). For each chain tested, Eq. (9) is numerically resolved with the parameters κ and κ_m, respectively, calculated from Eqs. (3) and (5), with the correct number N of endosomes in the chain, the applied magnetic field B, and the corresponding magnetic susceptibility.

To investigate the occurrence of shear-thinning or shear-thickening effects inside the cell, response curves to successive step-field pulses were measured for the same chains. Five successive rotational response curves for one identical chain are illustrated in Fig. 8(a), showing no significant differences and leading to very close viscoelastic parameters deduced from the best fits using Eq. (9). Then, to study a possible deviation from linear mechanical behavior, four different initial torques were applied to the same chains: the magnetic field is varied from 23 to 55 mT and the mechanical torque per chain volume (specific torque) ranges from 30 to 200 Pa. The average shear stress is then found between 50

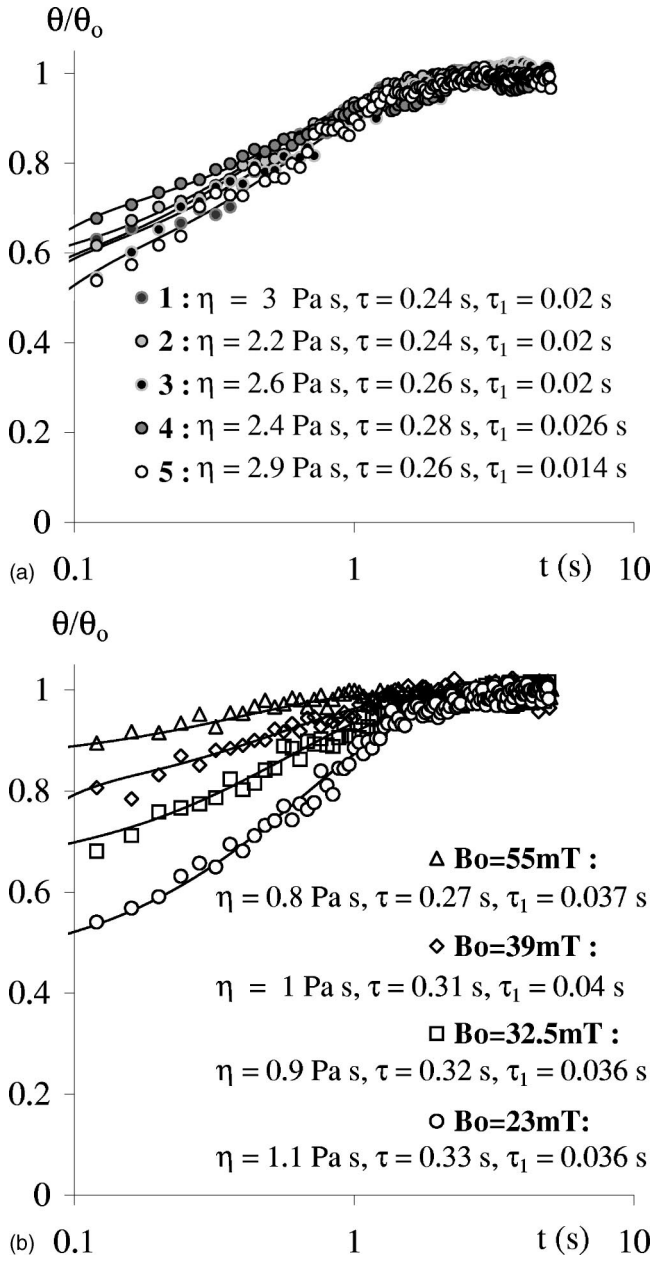

FIG. 8. (a) Five successive rotations of a unique chain. For each angular response curve, the best fit is superimposed (black line). The viscoelastic parameters deduced do not significantly vary from the first imposed rotation to the following ones. We find $\eta=2.6\pm0.4$ Pa s, $\tau=0.26\pm0.02$ s, $\tau_1=0.02\pm0.004$ s. (b) Angular response curves, with the corresponding fits (black lines) for the same chain submitted to increasing applied magnetic field (from 23 to 55 mT). The deduced viscoelastic parameters do not depend on the initial applied torque, with mean values $\eta=0.95\pm0.15$ Pa s, $\tau=0.31\pm0.04$ s, $\tau_1=0.037\pm0.003$ s.

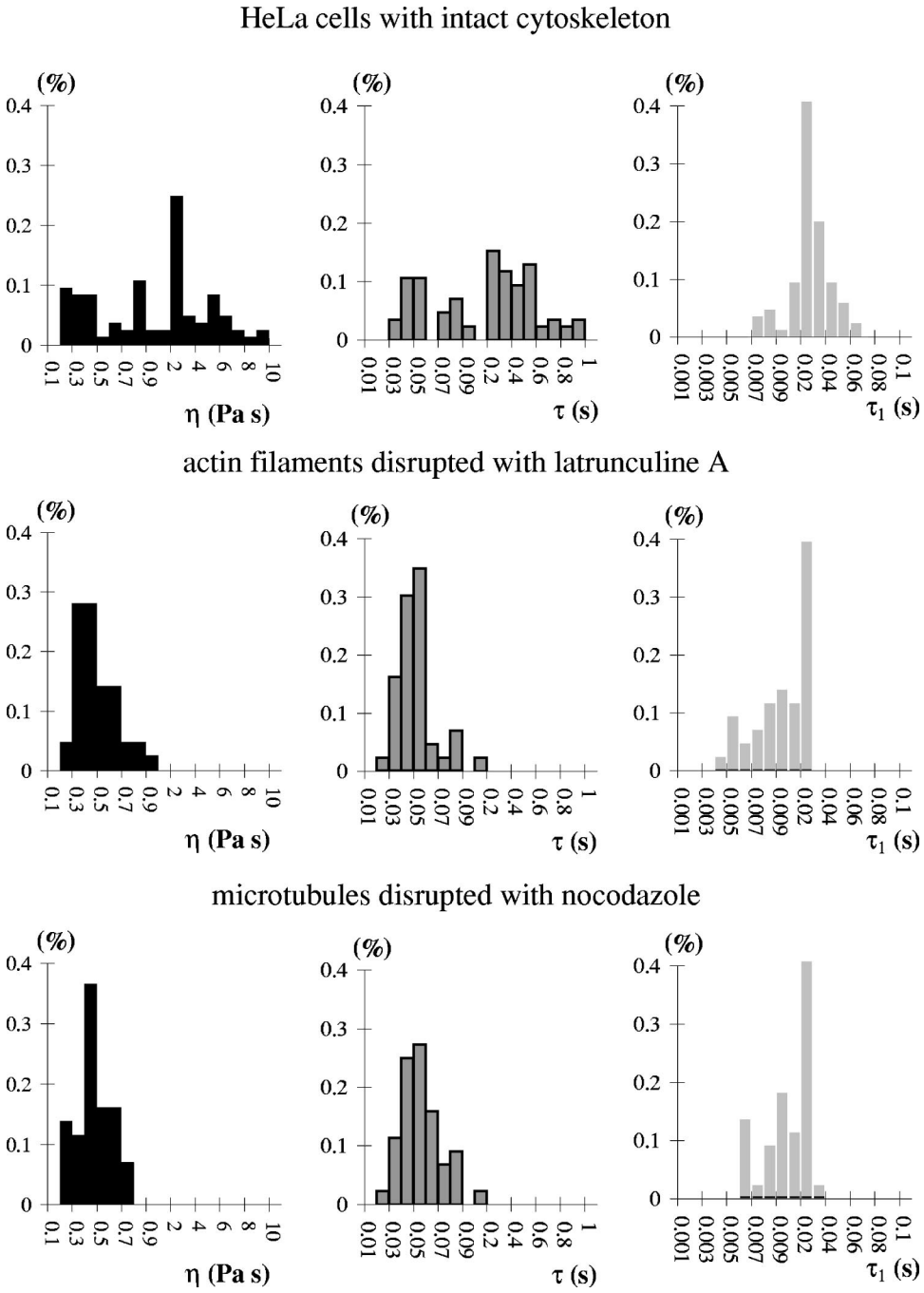

FIG. 9. Distribution of the viscoelastic parameters η, τ, and τ_1 measured in cells with an intact cytoskeleton and in cells treated with either latrunculine A or nocodazole. In intact cells, the distribution is obtained from measurement of 80 viscoelastic parameters, each set of parameters corresponding to the microenvironment of a different chain. In cells treated with cytoplasmic drugs, 40 different chains were analyzed for each condition. Note the difference of scale. The main effects of the disruption of either actin filaments or microtubules are the narrowing of the distribution of the viscoelastic parameters and the suppression of dense viscoelastic regions.

Pa (chains of four endosomes submitted to a 23 mT magnetic field) and 400 Pa (chains of two endosomes submitted to a 55 mT magnetic field). An example of the four rotational response curves obtained for one chain is illustrated in Fig. 8(b), with the corresponding fits obtained from Eq. (9). The viscoelastic parameters deduced from the fits are found to be constant over a wide range of specific torque amplitudes. Therefore, under our experimental conditions, the cell interior behaves as a Newtonian body.

The rotation of 80 distinct chains inside different HeLa cells with intact cytoskeleton and 40 different chains when actin filaments or microtubules are disrupted has been analyzed in terms of the three viscoelastic parameters η, τ, and τ_1. The distributions of these three parameters are illustrated in Fig. 9. First, we note that the viscoelasticity exhibits large dispersion as a function of the chain localization inside the cells with an intact cytoskeleton. Moreover, we observed that dense viscoelastic microenvironments (corresponding to a viscosity up to 10 Pa s and a relaxation viscoelastic time which reaches 1 s) correspond mostly to chains located in the center of the cell, near the nucleus, whereas most of the chains located farther from the nucleus suffer lower viscosity and relaxation time (with values that can fall down to 0.2 Pa s for the viscosity and 0.04 s for the relaxation time). We can deduce an average set of viscoelastic parameters describing the global mechanical properties of the cell interior: $\eta = 2.1 \pm 2$ Pa s, $\tau = 0.25 \pm 0.23$ s, and $\tau_1 = 0.02 \pm 0.01$ s. When either actin filaments or microtubules are disrupted,

the local viscoelasticity becomes more homogeneous (see Fig. 9) as a function of intracellular localization, with mean values $\eta = 0.43 \pm 0.17$ Pa s, $\tau = 0.043 \pm 0.017$ s, and $\tau_1 = 0.01 \pm 0.004$ s for cells treated with latrunculine A, and $\eta = 0.4 \pm 0.14$ Pa s, $\tau = 0.048 \pm 0.016$ s, and $\tau_1 = 0.011 \pm 0.004$ s for cells treated with nocodazole.

V. DISCUSSION

A. Rotational microrheology in living cells

The spontaneous endocytosis of anionic magnetic nanoparticles leads to the formation of endogeneous magnetic endosomes within the cell cytoplasm that can be monitored with an external magnetic field as a control parameter. First, the intracellular magnetic probe results from the endocytosis process rather than phagocytosis and broadens to a wide range of cell lines the possibility of monitoring magnetic organelles. Second, endosomal magnetic labeling allows one to obtain relevant information about the organization of their surrounding medium: in this study, we use the technique developed in [22] to mechanically characterize the endosome microenvironment. The directed local rotation of chains of endosomes, observed on a short temporal scale with ultrarapid videomicroscopy, reveals the local viscoelastic properties of the medium surrounding the chains. By optical microscopy, it is difficult to detect magnetic endosomes. Compared to microbeads contained within phagosomes, used for example in [21], endosomes are smaller and easily confused with other organelles of the cell cytoplasm. The use of fluorescent magnetic nanoparticles for endosomal labeling could overcome this obstacle and allow on to probe the cell cytoplasm by translating fluorescent magnetic endosomes. Nevertheless, fluorescence microscopy does not allow one to study short time dynamics, which is crucial for the determination of elasticity. These limitations motivated the choice of working on small chains of endosomes formed in a permanent magnetic field and easily recognizable. In response to rapid rotation (in less than 1 μs), the chains rotate inside the cell cytoplasm and their dynamics is governed by the viscoelasticity of their microenvironment. Moreover, the rotation of the chain is observed with a time resolution up to 2 ms, allowing one to catch the initial fast elastic response. This approach to measuring intracellular mechanical properties offers critical advantages: the use of an endogeneous and biologically functional probe, the temporal resolution, and the micrometric spatial range of the measurement.

B. Generality of the Maxwell liquid model for the viscoelasticity of the cell interior

The rotational microrheology method is grounded in the analysis of the rotational response in terms of a simple mechanical equivalent circuit composed of suitable arrays of two elementary elements, dashpot and spring. To understand the significance and generality of the linear equivalent circuits that have been used to describe the cell viscoelasticity, one must distinguish the techniques achieving cell deformation through manipulations at the cell surface from the purely intracellular rheological methods. Whole-cell deformation is generally explained by the association of a permanent tension or an elastic spring, accounting for the contributions of both the plasma membrane and the cortical cytoskeleton, in parallel with a Maxwell circuit modeling the cell interior [26,27,4,28,29]. The prevalent model for cytoplasm rheological behavior is therefore a viscoelastic liquid, represented by the Maxwell model. At short times (high frequency), the dynamics is dominated by elasticity, whereas at long times (low frequency), the medium behaves as a pure viscous liquid. The opposite behavior (viscoelastic solid or liquid at short times and solid at long times) is represented by the Voigt model (spring and dashpot in parallel). When the cytoplasm viscoelasticity is probed from inside the cell by analyzing the response of an intracellular bead to an applied stress [21,20,30], an extension of the Maxwell model (Kelvin-Maxwell or Voigt-Maxwell models) is needed to account for the local dissipation during the initial elastic deflection of the bead. In the present study, the Voigt-Maxwell model is actually the simplest configuration of viscoelastic parameters that fits the experimental curves with remarkable accuracy. The Voigt element (G, η_1) is responsible for the elastic response at short times: during the corresponding characteristic time $\tau_1 = \eta_1 / G$, the matrix surrounding the chain behaves as a viscoelastic solid. The elastic stress then relaxes in a time $\tau = \eta / G$. After this relaxation, the microenvironment of the endosomes behaves just like a liquid with viscosity η. To compare this phenomenological model with rheological measurements that provide the frequency dependence of the complex viscoelastic modulus $G^*(\omega)$, one can write the equation of motion [Eq. (8)] in the complex Fourier domain and directly deduce the complex shear modulus equivalent to the Voigt-Maxwell model:

$$G^*(\omega) = G_d \exp i\delta = i\eta\omega \frac{1 + i\omega\tau_1}{1 + i\omega(\tau + \tau_1)}. \qquad (10)$$

The magnitude G_d is a measure of the cytoplasm's resistance to deformation and the phase lag δ is an index of the cytoplasm's solidlike ($\delta = 0$) or liquidlike ($\delta = \pi/2$) behavior as a function of frequency. The global magnitude and phase of the viscoelastic modulus describing the whole-cell interior can then be directly calculated from all the local viscoelastic parameters measured in HeLa cells (Fig. 9). They are both represented in Fig. 10 for intact cells and for cells treated with cytoplasmic drugs. Note that the relevance of the shear modulus is reduced to the frequency range (1–500 Hz) imposed by the time scale and resolution of the direct rotation measurement. Its high frequency behavior [almost liquidlike ($\delta = \pi/2$) and dominated by the ''microviscosity'' η_1] is characteristic of semiflexible polymer dynamics and reflects the local bending modes of the cytoskeleton networks. At low frequency, however, the cytoplasm exhibits a fully liquidlike behavior (effective viscosity η), which contrasts with the behavior of pure *F*-actin, which is solidlike [16] and dependent on filament length. In between, δ shows a minimum, revealing a viscoelastic behavior. The effect of cytoskeletal drugs in the perinuclear region appears as a decrease in magnitude G_d and a more liquidlike behavior at low frequency.

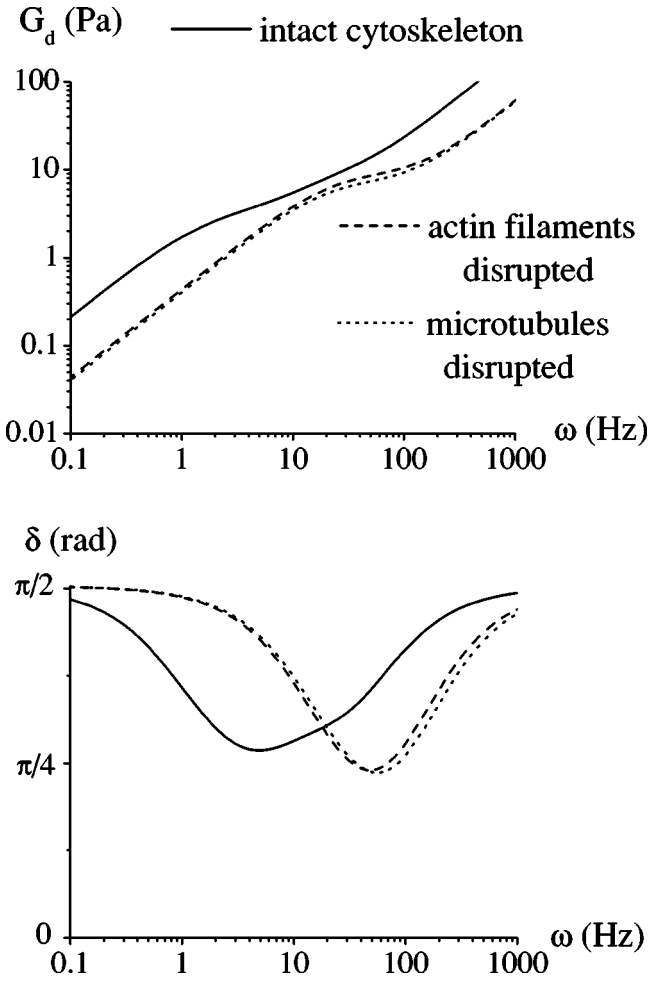

FIG. 10. Global frequency dependent modulus G_d (above) and phase δ (below) of the equivalent complex shear modulus describing the interior of HeLa cells, treated or not with cytoplasmic drugs, deduced from the entire sets of measured local viscoelastic parameters.

C. Implications for the cytoarchitecture

Under our experimental conditions (time scale 0.002–1 s, perturbation on the micrometer scale, specific applied torques ranging from 30 to 200 Pa), the cell interior behaves as a Newtonian body. This behavior was previously found for macrophages in [21] with similar experimental conditions, or in [15] where ferrimagnetic microbeads bound to integrin receptors on the surface of muscle cells were magnetically twisted. In the last study, the cortical cytoskeleton and the cytoplasm were deformed together with specific torque amplitudes 1.8–130 Pa, close to the ones applied in the present work.

In intact cells, the viscoelastic parameters exhibit a high degree of heterogeneity with a relaxation time τ differing by one order of magnitude between different subregions of the cell interior. On the whole, chains with perinuclear localization appear firmly entrapped in a rigid mesh characterized by $\eta=3.2$ Pa s and $\tau=0.4$ s, although most of the chains located farther from the center of the cell rotate more easily, yielding $\eta=0.4$ Pa s and $\tau=0.05$ s. By averaging all the locally measured viscoelasticities, one finds the mean viscosity $\eta=2.1$ Pa s and relaxation time $\tau=0.25$ s inside cells with an intact cytoskeleton. When one type of cytoskeletal filament (filamentous actin or microtubules) is disrupted, the whole cytoplasm is found to exhibit roughly the same rheological properties, whatever the intracellular localization of the probed chains within the cell. The corresponding mean viscoelastic parameters fall to $\eta=0.43$ Pa s, $\tau=0.043$ s when actin filaments are disrupted and to $\eta=0.4$ Pa s, $\tau=0.048$ s when microtubules are disrupted, close to the values obtained in regions far from the nucleus inside intact cells. One must note that the conditions of the selective depolymerization rupture of either microtubules or actin filaments may lead to a reorganization of the remaining cytoskeleton filaments. The similar decrease of the measured viscoelasticities whether actin filaments or microtubules are disrupted suggests that the microenvironment of the chains is no longer dependent on the presence of microtubules or actin filaments and reflects the cytoplasm content (cytosol, mitochondria, endoplasmic reticulum, and Golgi membranes). Hence the measured viscoelasticities provide relevant insight into the cytoarchitecture: chains located near the nucleus are embedded in a relatively rigid viscoelastic material whereas the others are surrounded by a softer viscoelastic material. The same measurement when one compound of the cytoskeleton is disrupted (actin filaments or microtubules) demonstrates that the dense viscoelastic perinuclear subregion is due to a cooperation of both filamentous actin and microtubules.

At this stage of our understanding, it is tempting to postulate that the difference in local viscoelasticity as a function of the cytoplasmic region is correlated with the functional status of the endosomes considered. It is well established that the motility of endosomes along microtubules is a key requisite for endocytotic vesicle sorting (by allowing vesicle fission), for the connection between early and late endosomes, and for the long range active transport of late endosomes that meet in the pericentriolar region to fuse with lysosomes [31]. According to our findings, these highly mobile endosomes experience a soft viscoelastic medium. By contrast, in the perinuclear region, the endosome motility is reduced by a dense viscoelastic network, in which both actin filaments and microtubules cooperate. Thus both types of filaments may be implicated in the maintenance of the steady state distribution of late endosomes and lysosomes in order to favor fusion events between these two compartments and to regulate local delivery of internalized molecules to lysosomes. This hypothesis is in keeping with the results of [32], which demonstrate the role of actin filaments and one associated myosin in immobilizing lysosomes during their travel along microtubules. It is also in agreement with the observation of the inhibition of lysosomal degradation process when one impedes the confluence of endosomes near the centrosome [33].

D. Comparison with other intracellular investigations

Magnetometry experiments have initiated global measurements of intracellular viscosity on pulmonary macrophages having phagocytized micrometric ferromagnetic particles

[34,19,35]. Magnetic tweezer experiments have extended the use of a phagocytized magnetic microprobe to apply a local perturbation inside the cell. The response to step-force pulses of one individual magnetic phagosome inside a macrophage or amoeba is then analyzed in terms of an equivalent Maxwell-like mechanical circuit [21,30]. If the measured effective viscosities are about two orders of magnitude greater than the ones obtained in the present work, the relaxation times deduced, reflecting the proportion of fluidlike versus solidlike behavior of the medium surrounding the probes, are nevertheless comparable.

Intracellular granules (diameter $\sim 0.6\ \mu$m) have been successfully trapped by optical tweezers in the cytoplasm of locomoting neutrophils [18]. They were oscillated at frequencies from 0.3 to 3 Hz with a maximum force applied of 15 pN (maximum applied stress 13 Pa) and with an amplitude of 0.5 μm. This technique of microrheology involving optical forces closely matches the magnetic rotational microrheology conditions. The viscosity is found to be 0.4–0.2 Pa s in the body and trailing regions of the migrating neutrophil, with relaxation times around 0.4 s, in very good agreement with the quantitative values measured in the present work. In addition, the authors have distinguished two populations of granules, a free easily oscillating population that experiences a soft viscoelastic environment, and a complementary fixed population (too stiff to measure) that is strongly embedded in the cytoskeleton networks. When cytoskeletal drugs are added (cytochalasine D or nocodazole), the fraction of fixed versus free granules dramatically decreases, and all the granules exhibit the same rheological properties as the free granules in the control case. The authors propose to identify the free granules as exocytotic or secretory vesicles, whereas the fixed granules could correspond to vesicles performing lysosomal functions. This behavior is quite similar to the present measurements where endosomes embedded in a dense viscoelastic region are distinguished from endosomes entrapped in a relatively soft viscoelastic medium, presumably because of their different functioning status in the endocytotic pathway.

The Brownian motion of intracellular probes inside epithelial cells has been measured by laser tracking, in the absence of any external force applied, with subnanometer and near-microsecond resolutions [16]. The mean square displacement is analyzed in terms of a complex viscoelastic modulus $G^*(\omega)$ over a wide frequency bandwidth. The probes are rigid spherical lipid-storage granules that do not show active transport, localized both in the perinuclear region and in the actin-rich large, flat lamellae that is characteristic of the kidney epithelial COS7 cell lines with number one. These endogenous granules show subdiffusive behavior with submicronic displacement at all lag times (granules showing large Brownian excursions cannot be tracked by laser tracking microrheology). As for endosomes in Hela cells (see Fig. 10), the phase lag δ for the intracellular granules shows a nonmonotonic behavior with a minimum. Quantitatively, the authors find $G_d(1\ \mathrm{Hz}) \sim 8$ Pa, $\delta(1\ \mathrm{Hz}) \sim 0.3\pi$, in good agreement with the values deduced from the phenomenological mechanical model describing the HeLa cell interior: $G_d(1\ \mathrm{Hz}) \sim 4.4$ Pa and $\delta(1\ \mathrm{Hz}) \sim 0.27\pi$. In conclusion, rotational microrheology reveals a viscoelastic behavior that is very similar to the one deduced from laser tracking of passive granules.

The comparison between the different studies probing the mechanical properties of the cytoplasm provides insights into the crucial parameters for the biological significance of the measurements. First, the techniques used can either measure the spontaneous motion of intracellular probes or use an external force to constrain the probe movement. Second, the choice of the intracellular probe is critical. Obviously, its size determines the spatial range of the microenvironment probed, but more important is the functional status of the probe within the cell. The distribution and dynamical behavior of various subcellular organelles (storage granules versus secretory vesicles, for example) are governed by their role in cell functioning or by the destination of their content. The microenvironment can be modulated by the recruitment of cytoskeletal filament and/or binding proteins with the view of achieving a specific process (fission, fusion, etc.). Interactions of the organelles with molecular motors are dictated by the need for long range transport or transient pause. Thus the microrheological intracellular measurements must be understood in relation to the complex machinery of intracellular traffic. The rotational magnetic endosome microrheology technique therefore has relevance for a better understanding of intracellular dynamics, as, for instance, to probe very local variations in the cytoskeletal architecture and to identify the roles of cytoskeletal proteins in relation to endocytotic compartments.

ACKNOWLEDGMENTS

We acknowledge S. Marion for crucial and major help in performing the immunofluorescence assay. We are grateful to E. Coudrier for fruitful discussions, J. Servais for technical assistance, C. Villiers for his teaching in endosome purification, and S. Neveu for providing us with the magnetic nanoparticles. This work was supported by the CNRS program Physique et Chimie du Vivant.

[1] O. Thoumine and A. Ott, Cell Motil. Cytoskeleton **35**, 269 (1996).
[2] R.M. Hochmuth, J. Biomech. **33**, 15 (2000).
[3] E. Evans, Biophys. J. **43**, 27 (1983).
[4] E.A. Evans and A. Yeung, Biophys. J. **56**, 151 (1989).
[5] R.M. Hochmuth, J. Biomech. Eng. **115**, 515 (1993).
[6] O. Thoumine and A. Ott, J. Cell. Sci. **110**, 2109 (1997).
[7] J. Guck, R. Ananthakrishnan, H. Mahmood, T.J. Moon, C.C. Cunningham, and J. Käs, Biophys. J. **81**, 767 (2001).
[8] T.J. Dennerll, P. Lamoureux, R.E. Buxbaum, and S.R. Heidemann, J. Cell Biol. **109**, 3073 (1989).
[9] N.O. Petersen, W.B. McConnaughey, and E.L. Elson, Proc.

Natl. Acad. Sci. U.S.A. **79**, 5327 (1982).
[10] J.H. Hoh and C.-A. Schoenenberger, J. Cell. Sci. **107**, 1105 (1994).
[11] M. Radmacher, M. Fritz, C.M. Kacher, J.P. Cleveland, and P.K. Hansma, Biophys. J. **66**, 2159 (1996).
[12] S. Hénon, G. Lenormand, A. Richert, and F. Gallet, Biophys. J. **76**, 1145 (1999).
[13] A.R. Bausch, F. Ziemann, A.A. Boulbitch, K. Jacobson, and E. Sackmann, Biophys. J. **75**, 2038 (1998).
[14] G.N. Maksym, B. Fabry, J.P. Butler, D. Navajas, D.J. Tschumperlin, J.D. Laporte, and J.J. Fredberg, J. Appl. Physiol. **89**, 1619 (2000).
[15] B. Fabry, G.N. Maksym, J.P. Butler, M. Glogauer, D. Navajas, and J.J. Fredberg, Phys. Rev. Lett. **87**, 148102 (2001).
[16] S. Yamada, D. Wirtz, and S.D. Kuo, Biophys. J. **78**, 1736 (2000).
[17] A. Caspi, R. Granek, and M. Elbaum, Phys. Rev. Lett. **85**, 5655 (2000).
[18] M. Yanai, J.P. Butler, T. Suzuki, A. Kanda, M. Kurachi, H. Tashiro, and H. Sasaki, Am. J. Physiol. **277**, C432 (1999).
[19] P.A. Valberg and H.A. Feldman, Biophys. J. **52**, 551 (1987).
[20] W. Möller, I. Nemoto, T. Matsuzaki, T. Hofer, and J. Heyder, Biophys. J. **79**, 720 (2000).
[21] A.R. Bausch, W. Möller, and E. Sackmann, Biophys. J. **76**, 573 (1999).
[22] C. Wilhelm, J. Browaeys, A. Ponton, and J.-C. Bacri, Phys. Rev. E **67**, 011504 (2003).
[23] C. Wilhelm, F. Gazeau, and J.-C. Bacri, Eur. Biophys. J. **31**, 118 (2002).
[24] S. Melle, G. Fuller, and M.A. Rubio, Phys. Rev. E **61**, 4111 (2000).
[25] C. Wilhelm, F. Gazeau, J. Roger, J.-N. Pons, and J.-C. Bacri, Langmuir **18**, 8148 (2002).
[26] G.W. Schmidt-Schönbein, K.L. Sung, H. Tözeren, R. Skalak, and S. Chien, Biophys. J. **36**, 243 (1981).
[27] C. Dong, R. Skalak, K.L.-P. Sung, G.W. Schmid-Schönbein, and S. Chien, J. Biomech. Eng. **110**, 27 (1988).
[28] M. Sato, D.P. Theret, L.T. Wheeler, N. Ohshima, and R.M. Nerem, J. Biomech. Eng. **112**, 263 (1990).
[29] K.A. Ward, W.I. Li, S. Zimmer, and T. Davis, Biorheology **28**, 301 (1991).
[30] W. Feneberg, M. Westphal, and E. Sackmann, Eur. Biophys. J. **30**, 284 (2001).
[31] J.P. Luzio, B.A. Rous, N.A. Bright, P.R. Pryor, B.M. Mullock, and R.C. Piper, J. Cell. Sci. **113**, 1515 (2000).
[32] M.-N. Cordonnier, D. Dauzonne, D. Louvard, and E. Coudrier, Mol. Biol. Cell **12**, 4013 (2001).
[33] P.M. Novikoff, M. Cammer, L. Tao, H. Oda, R.J. Stockert, A.W. Wolkoff, and P. Satir, J. Cell. Sci. **109**, 21 (1996).
[34] P.A. Valberg and D.F. Albertini, J. Cell Biol. **101**, 130 (1985).
[35] W. Möller, S. Takenaka, M. Rust, W. Stahlhofen, and J. Heyder, J. Aerosol Med. **10**, 173 (1997).